Shape of an elastic loop strongly bent by surface tension: Experiments and comparison with theory

Serge Mora,[1,*] Ty Phou,[1] Jean-Marc Fromental,[1] Basile Audoly,[2] and Yves Pomeau[3]
[1]*Laboratoire Charles Coulomb, UMR 5221, Université Montpellier 2 and CNRS, Place Eugène Bataillon, F-34095 Montpellier Cedex, France*
[2]*CNRS and UPMC Université Paris 06, UMR 7190, Institut Jean le Rond d'Alembert, Paris, France*
[3]*Department of Mathematics, University of Arizona, Tucson, Arizona 85721, USA*
(Received 22 June 2012; published 30 August 2012)

When a very flexible wire is dipped into a soapy solution, it collapses onto itself. We consider the regions of high curvature where the wire folds back onto itself, enclosing a capillary film. The shapes of these end loops are measured in experiments using soap films and compared to a known similarity solution. The sizes of these structures provide a simple and reliable way to measure surface tension.

DOI: 10.1103/PhysRevE.86.026119 PACS number(s): 89.90.+n, 46.25.−y, 46.32.+x, 68.03.Cd

I. INTRODUCTION

When a long and flexible wire such as a hair strand is dipped into a soapy solution, capillary attraction can make the wire collapse onto itself. Near the end, a region of large curvature is formed where a small, closed loop encloses a capillary film (see Fig. 1). The shape of the loop, called an "end loop" hereafter, results from the balance of the capillary forces, which tend to shrink the loop, and the elastic bending forces, which resist curvature. This end loop can be observed when the elastocapillary length (see below) is significantly smaller than the length of the wire: the planar configuration wherein a disklike capillary films rests on a circular loop is then unstable [1]. For increasing surface tension, it successively bifurcates to a planar oval shape, to a twisted saddlelike surface, to a figure-of-eight shape having a point of self-contact, and then to a configuration made up of two end loops connected by a line of self-contact [2].

One interesting feature of the end loop is that it is described by a similarity solution. The elasticity of the wire and the capillary attraction give rise to a length scale known as the elastocapillary length [3,4]. When this natural length is used, the equations and boundary conditions for the shape of the end loop are free of any parameter. As a result, its shape is universal up to a global change of scale [5]. (In particular, the total length of the wire has no influence on the end loop as any length in excess is absorbed into the segment with self-contact which acts like a reservoir.) We carried out experiments using soap films and compare the observed shapes to the analytical solution. Measuring the size of the end loop provides a simple and reliable way to measure the surface tension of the fluid knowing the bending modulus of the wire.

Since the work of Lagrange and Plateau [6], the equilibrium shape of a soap film resting on a rigid frame specified by a three-dimensional (3D) curve is known to be selected by minimization of the surface area. Since then, there has been a considerable amount of work on minimal surfaces in various areas of science, including the geometry of surfaces and the fluid mechanics of soap films. For the problem at hand, we only consider planar configurations of the enclosing frame: then the shape of the film is readily found as it is just the domain enclosed by the wire in its plane.

The capillary film deforms the wire by applying a force per unit length in the direction perpendicular to the wire and contained in the plane of the film. The equations governing the equilibrium of the flexible wire are then identical to those for the collapse of a cylindrical shell under external pressure. This problem of a closed 2D elastic ring subjected to a distributed normal force has a long history. At the end of the 19th century, Lévy [7] reduced the investigation of post-buckled solutions to an algebraic problem involving elliptic integrals. More than half a century later, Carrier [8] reconsidered this problem and solved the case of small deformations near the onset of buckling; his analytical work was later extended by Adams [9]. Tadjbakhsh and Odeh [10], followed by several other authors, solved the boundary-value problem numerically and determined the post-buckled shapes. Self-contact was first considered by Flaherty [5], who reports that in the planar setting and for increasing values of the pressure, the ring first makes a single point of self-contact and later develops contact along a segment, then forming a two-headed racket-like structure (end loops). They also derived the similarity equations describing these end loops and solved them by a nonlinear shooting method. Recently, a breakthrough was achieved by Djondjorov and collaborators [11], who solved the post-buckled shapes of the elastic ring subjected to external pressure in a completely analytical manner. They considered configurations having extended self-contact along a line but wrongly assumed that the shape of each end loop is given by scaling down the figure-of-eight solution having a pointlike contact as obtained *at the onset of contact*; as a result, their solution displays a nonphysical discontinuity of moment at the edge of the region of contact and differs from the numerical one of Flaherty that is the correct one. The correct sequence of shapes produced by a progressive increase of the external pressure is as follows. At the onset of contact, the curvature at the point of contact is nonzero, and the force of contact is zero. Then, the curvature at the point of contact progressively decreases, and the force increases. When this curvature cancels, it stays at zero, and the pointlike region of contact becomes a line.

Here, we modify the beautiful analytical solution of Djondjorov, using the correct condition at the edge of the loop. It is consistent with the numerical solution of Flaherty but is

*smora@univ-montp2.fr

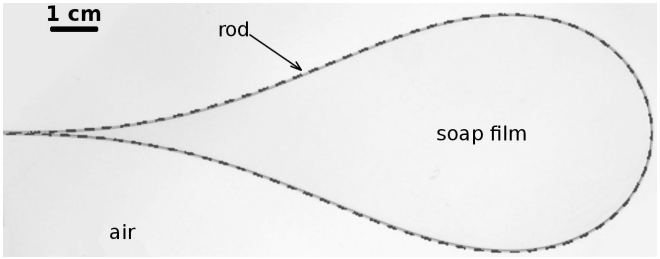

FIG. 1. A rod enclosing a film of a commercial dishwashing liquid. The Young modulus of the rod is $E = 3.55 \pm 0.1$ GPa, the radius is $\rho = 0.25$ mm, and the surface tension of the film is $\sigma = 27.3$ mN/m. The dashed curve is the theoretical prediction scaled with Eq. (1) (no fitting parameter).

considerably simpler as it does not require nonlinear shooting. (Our implementation of the numerical solution is provided in Fig. 5.) Note that a variant of our problem, wherein the capillary film has been pierced and a capillary bridge extends along the segment of contact only, has been analyzed based on order of magnitude arguments in Ref. [12] and solved numerically in Ref. [13].

II. EXPERIMENTS

We have used nylon fishing lines with different diameters (2ρ), ranging from 0.25 mm to 0.5 mm. Using a tensile testing machine, we observed a linear dependence of the stress with the elongation for stresses less than 2% and determined the Young's modulus $E \simeq 3.55 \pm 0.1$ GPa. No irreversible deformation was observed in tests that were shorter than ten seconds and with elongation less than 2%. Note that these wires being obtained by extrusion, their mechanical properties are expected to be anisotropic. The measured Young's modulus is then the longitudinal one, which is precisely the one relevant to the calculation of the bending modulus ($\frac{\pi}{4} E\rho^4$). In the experiments presented below in which the rod is bent by the action of capillary forces, we have checked that the maximal curvature R of the rod is such that $\rho/R < 1.3\%$, so the material stays in the linear regime. In these experiments, the rod is first stretched and then heated up to 60 °C, a temperature slightly lower than the glass transition temperature of nylon, for a few minutes. This removes any residual natural curvature in the wire. Held by its ends, the rod is immersed in a solution of surfactant molecules and then gently removed so that a soap film is enclosed by a loop (see Fig. 1). The wire recovers an almost straight shape when released, provided the film exists for no more than about ten seconds. Here, "almost straight" means having a final radius of curvature at least ten times larger than that in the presence of the soap film. Each experiment was performed with a new and perfectly straight rod.

The surface tension of a soap film essentially depends on the nature of the surfactant molecules, their concentration, the solvent (pure water, brine, etc.), and the temperature. Surfactants used in this study are commonly used nonionic and ionic detergents. They include Brij 30 [$C_{12}H_{25}(O–CH_2–CH_2)_4OH$], Brij 58 [$C_{16}H_{33}(O–CH_2–CH_2)_{20}OH$], Brij 700 [$C_{18}H_{37}(O–CH_2–CH_2)_{100}OH$], Triton X100 (TX 100) [$C_{14}H_{21}O(CH_2–CH_2–O)_{10}H$], cetylpyridinium chloride (CpCl) (from Aldrich), and a commercial dishwashing liquid. The water used was

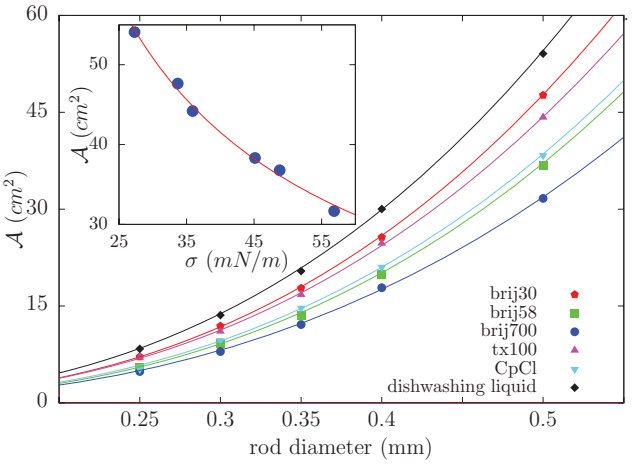

FIG. 2. (Color online) Measured end-loop area $\mathcal{A}$ as a function of the wire diameter for suspended films with surfactant concentrations above the CMC. The lines indicate the best fits for $\mathcal{A} = ax^b$. One finds $b = 2.72 \pm 0.04$ for Brij 30, 2.74 ± 0.04 for Brij 58, 2.65 ± 0.03 for Brij 700, 2.68 ± 0.03 for TX 100, 2.71 ± 0.05 for CpCl, and 2.69 ± 0.03 for the dishwashing liquid. Inset: The loop area $\mathcal{A}$ as a function of the surface tension for a wire with a radius $\rho = 0.25$ mm. The line indicates the best fit for $\mathcal{A} = cx^d$. One finds $d = -0.69 \pm 0.03$.

ultrapure (18 MΩ cm). Surface tension is known to decrease as the surfactant concentration increases in water and to stabilize beyond the critical micelle concentration (CMC) [14]. Depending on the surfactant, the surface tension beyond the CMC ranged in these experiments from ∼27 to ∼57 mN/m. It was measured by the drop detachment method. The accuracy of our surface tension measurements is better than 0.5%, and we find $\sigma = 33.7$ mN/m for Brij 30, 48.8 mN/m for Brij 58, 56.9 mN/m for Brij 700, 35.9 mN/m for TX 100, 45.1 mN/m for CpCl, and 27.3 mN/m for the dishwashing liquid we used.

A typical experimental shape of an end loop enclosing a thin fluid film is superimposed to the analytical solution derived later in Fig. 1. We repeated this experiment using the different surfactants and different rod diameters. To maximize the accuracy of the measurements, we measured the areas of the loops and not their widths or heights. The measured area $\mathcal{A}$ is found to be proportional to the radius of the wire to the power 2.70 ± 0.3 and to the surface tension of the film to the power -0.69 ± 0.03 (see the inset of Fig. 2).

Estimating a film thickness of 10 μm, the elastogravity number, defined as the ratio of gravitational energy (roughly defined as the total weight times half of the loop length) and the bending energy, is found to range (depending on the surface tension and/or the rod radius) between 10^{-3} and 0.05. Gravity can thus be neglected in these experiments.

III. THEORY

Here, we derive a solution for a planar elastic ring subjected to a normal force having constant magnitude. This problem was solved by a nonlinear shooting method by Flaherty [5]. Our solution is based on the recent analytical solution of Djondjorov [11], which is both more elegant and much easier to implement numerically. (Instead of nonlinear shooting, we shall only need to solve a set of nonlinear equations.)

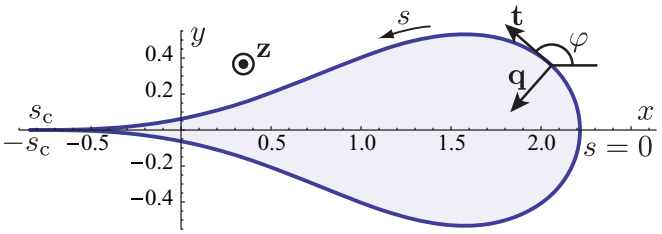

FIG. 3. (Color online) Notations relevant to the analysis of planar solutions of the elastica problem. The configuration shown is the solution for an end loop, using coordinates rescaled by the elastocapillary length ℓ_{ec}.

We correct the original solution of Djondjorov and use the appropriate condition of vanishing curvature at the edge of the region of contact.

We first make lengths dimensionless using the elastocapillary length [3,4]

$$\ell_{ec} = \left(\frac{B}{2\sigma}\right)^{1/3}, \tag{1}$$

where $B = \frac{\pi\rho^4 E}{4}$ is the bending modulus. In rescaled variables, both the bending modulus and the surface tension are effectively equal to one.

We use the geometric notations shown in Fig. 3. Let x and y denote the Cartesian coordinates, s the arclength, $\mathbf{t} = (\cos\varphi, \sin\varphi)$ the unit tangent, and $\mathbf{q} = (-\sin\varphi, \cos\varphi)$ the unit normal. Let $\mathbf{a}$ and $\mathbf{b}$ be any pair of vectors in the plane. The cross product of two such vectors is the *scalar* $\mathbf{a} \times \mathbf{b} = a_x b_y - a_y b_x$. The cross product of the normal unit vector $\mathbf{z}$ and an in-plane vector $\mathbf{a}$ denotes the *vector* obtained by a rotation of $\pi/2$, namely, $\mathbf{z} \times \mathbf{a} = (-a_y, a_x)$.

Following the classical elastica theory, the internal stress in the elastic ring is represented by the resultant $\mathbf{n}(s)$ and its moment $m(s)$ about the z axis. Then the local balance of moments is $m'(s) + \mathbf{t}(s) \times \mathbf{n}(s) = 0$. Solving for $\mathbf{n}$, this yields $\mathbf{n}(s) = T(s)\mathbf{t}(s) - m'(s)\mathbf{q}(s)$, where $T(s) = \mathbf{n}(s) \cdot \mathbf{t}(s)$ is the yet unknown scalar tension. In rescaled variables, the constitutive law is $m(s) = \kappa(s)$, where $\kappa(s) = \varphi'(s)$ is the curvature. We, therefore, have

$$\mathbf{n}(s) = T(s)\mathbf{t}(s) - \kappa'(s)\mathbf{q}(s). \tag{2}$$

The balance of forces is $\mathbf{n}'(s) + \mathbf{q}(s) = \mathbf{0}$, where the unit normal $\mathbf{q}$ in the second term accounts for the capillary force exerted by the film, the value of the surface tension being 1 in our rescaled units. Inserting the expression for $\mathbf{n}$ just obtained, carrying out the derivative, and making use of the geometrical relations $\mathbf{t}' = \kappa\mathbf{q}$ and $\mathbf{q}' = -\kappa\mathbf{t}$, we find two equations. The first one reads $T' = -\kappa\kappa'$ and can readily be integrated as

$$T(s) = -\frac{\kappa^2(s)}{2} + \mu, \tag{3}$$

where μ is a constant of integration. The second equation then yields [7]

$$-\kappa''(s) - \frac{\kappa^3(s)}{2} + \mu\kappa(s) + 1 = 0. \tag{4}$$

Note that the last term in this equation is the surface tension, whose value is $1/2$ in our rescaled units.

It is well known that the solution for the end loop is symmetric [15], and we choose to align the x coordinate axis with the axis of symmetry. At the point $s = s_c$ where the ring closes up onto itself, the following conditions hold:

$$y(s_c) = 0, \quad \varphi(s_c) = \pi, \quad \kappa(s_c) = 0. \tag{5}$$

The first two conditions come from symmetry. The last condition is the so-called Weierstrass-Erdmann corner condition: in the presence of a moving boundary and without adhesion, the bending moment is continuous across the edge of the region of contact [16,17], and therefore, the curvature goes to zero. This condition is not satisfied by Djondjorov's solutions.

Using the geometrical identity $\mathbf{q}(s) = \mathbf{z} \times \mathbf{t}(s)$ and the condition of inextensibility $\mathbf{r}'(s) = \mathbf{t}(s)$, the balance of force $\mathbf{n}'(s) + \mathbf{q}(s) = \mathbf{0}$ can be integrated as $\mathbf{n}(s) = -\mathbf{z} \times [\mathbf{r}(s) - \mathbf{r}_0]$, where $\mathbf{r}_0$ is a constant of integration, called the center of forces. By symmetry, this $\mathbf{r}_0$ lies on the axis of symmetry. Setting the origin of the coordinate system at this point, we have $\mathbf{r}_0 = \mathbf{0}$. Then, $\mathbf{n}(s) = -\mathbf{z} \times \mathbf{r}(s)$, and so

$$\mathbf{r}(s) = \mathbf{z} \times \mathbf{n}(s). \tag{6}$$

At the point of contact $s = s_c$, where $y(s_c) = 0$, the above equation implies $n_x(s_c) = 0$. There, $\mathbf{t}(s_c) = (-1,0)$, and so $T(s_c) = \mathbf{n} \cdot \mathbf{t} = -n_x = 0$. Combining this with Eq. (3) and with the condition $\kappa(s_c) = 0$, this shows that the constant of integration μ vanishes for an end-loop solution connecting to an extended region of contact, so

$$\mu = 0. \tag{7}$$

Solutions to Eq. (4) that are even functions of s are of the form

$$\kappa(\mathbf{c},s) = c_1 + \frac{c_2}{c_3 + cn[c_4 s - 2K(c_5), c_5]}, \tag{8}$$

where c_i are constants, cn is the Jacobi elliptic function, and K denotes the complete elliptic integral of the first kind. This expression comes from Eq. (38) of Ref. [11]; we have included a new contribution $-2K(c_5)$ in the argument of the Jacobi cn function that warrants symmetry, so $\kappa(\mathbf{c},s) = \kappa(\mathbf{c}, -s)$. This is because we define the origin of an arclength to be at the apex of the loop as shown in Fig. 3. The five constants $\mathbf{c} = (c_1, \ldots, c_5)$ are subjected to two types of conditions: (i) the function $\kappa(\mathbf{c},s)$ must actually be a solution of the differential Eq. (4) with $\mu = 0$—as not all of them are, and (ii) it must satisfy the boundary conditions of Eq. (5).

Analytical expressions for the generic sets of parameters $\mathbf{c}$ that satisfy condition (i) are available in Ref. [11], but they depend on a series of intermediate quantities defined by cumbersome expressions. We found it much more convenient to bypass these expressions and instead enforce the differential Eq. (4) at a few selected points:

$$2\kappa''(\mathbf{c},0) + \frac{\kappa^3(\mathbf{c},0)}{2} = 2 \tag{9a}$$

$$2\kappa''(\mathbf{c},1) + \frac{\kappa^3(\mathbf{c},1)}{2} = 2 \tag{9b}$$

$$2\kappa''(\mathbf{c},2)+\frac{\kappa^3(\mathbf{c},2)}{2}=2 \tag{9c}$$

$$2\kappa''(\mathbf{c},3)+\frac{\kappa^3(\mathbf{c},3)}{2}=2. \tag{9d}$$

Here, we have chosen, somewhat arbitrarily, to make use of the integer points $0 \leqslant s \leqslant 3$, but almost any other choice is possible, and the final result is independent of this choice of values of s. This yields four equations for the five parameters $(c_1,\ldots,c_5)$. A simple counting argument shows that this is consistent: the second-order Eq. (4) together with condition (7) and the symmetry condition $\kappa'(0)=0$ spans a one-parameter family of solutions.

We still need to use condition (ii) that holds at the edge of the region of contact [see Eq. (5)] except for the condition $y(s_c)=0$ that has already been used to prove $\mu=0$. Recalling the definition of curvature $\kappa=\varphi'$, the second condition $\varphi(s_c)=\pi$ can be rewritten as an equation for the parameters $\mathbf{c}$ and s_c:

$$\int_0^{s_c}\kappa(\mathbf{c},s)ds=\frac{\pi}{2}. \tag{10}$$

In this equation, the trial form of κ proposed in Eq. (8) is inserted, and the integral is computed symbolically in terms of special functions; an explicit expression for the integral can also be found in Ref. [11].

Our last equation is the last condition from Eq. (5):

$$\kappa(\mathbf{c},s_c)=0. \tag{11}$$

The six nonlinear Eqs. (9)–(11) are solved numerically for the five constants $c_1,\ldots,c_5$ and for the unknown coordinate s_c of the point of contact. An implementation using the FINDROOT function in WOLFRAM MATHEMATICA [18] is proposed in the Appendix. It yields the following root:

$$\mathbf{c}=\begin{pmatrix}-3.092\,023\,442\\ 11.617\,026\,404\,0\\ 3.235\,133\,312\,1\\ 1.255\,703\,024\,8\\ 0.133\,149\,136\,3\end{pmatrix},\quad s_c=3.421\,667\,768\,6. \tag{12}$$

The solution is plotted in Fig. 3 with the help of Eq. (6). It is graphically similar to the solution found by Flaherty [5] using nonlinear root finding. In rescaled units, the area of the end loop is

$$\mathcal{A}_{\rm th}=1.5609. \tag{13}$$

in the simulation.

IV. DISCUSSION

The experimental shapes of the end loops obtained using the different surfactants and wire diameters all match the predicted one within the camera accuracy (see Fig. 1). Furthermore, the scalings experimentally found for the loop area, i.e., $\mathcal{A}\propto\rho^{2.70\pm0.3}$ (Fig. 2) and $\mathcal{A}\propto\sigma^{-0.69\pm0.3}$ (inset of Fig. 2) agree with the dimensional analysis predicting that it depends on the wire radius as $\rho^{8/3}$ and on the surface tension as $\sigma^{-2/3}$. Moreover, Fig. 4 shows that the experimental data are in quantitative agreement with the theoretical prefactor of Eq. (13).

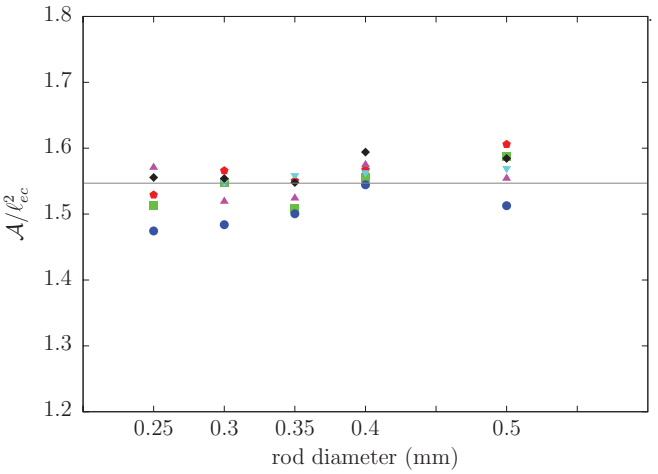

FIG. 4. (Color online) Area divided by $\ell_{\rm ec}^2$ as a function of the rod diameter for Brij 30 (pentagons), Brij 58 (squares), Brij 700 (circles), TX 100 (triangles up), CpCl (triangles down), and the dishwashing liquid (diamonds). Averaging and taking into account the uncertainties for measurements of Young's modulus and surface tensions, we find that $\mathcal{A}/\ell_{\rm ec}^2=1.55\pm0.04$. The solid line is the theoretical value from Eq. (13).

V. CONCLUSION

Strongly post-buckled shapes induced by a force normal to an elastic rod have been investigated—both experimentally and theoretically—by the means of capillary end loops. The agreement between the analytical solution we have obtained and measurements is quantitatively good.

Measuring the size of the end loop provides a direct and convenient way to measure either the bending modulus of a wire or the surface tension of a suspended film. Starting from a reference surfactant solution whose surface tension is known and from a given wire, or starting from a wire whose radius and Young's modulus are known, the determination of an unknown surface tension is straightforward using the above results. This provides a simple, accurate, and very cheap method to measure surface tension.

APPENDIX: A MINIMAL NUMERICAL SOLUTION

The solution for the end loop requires a numerical root finding. A numerical solution of the set of Eqs. (8)–(11) using WOLFRAM MATHEMATICA [18] is shown in Fig. 5 and requires fewer than ten lines of code. This solution is represented in Fig. 3.

```
kappa = Function[s, q1 + q2 / (q3 + JacobiCN[q4 s - 2 EllipticK[q5], q5])];
phi = Integrate[kappa[s], s] // Simplify // Function@@{s, #} &;
eqn = Function[s, 2 kappa''[s] + kappa[s]^3 - 2];
theSol = FindRoot[{eqn[0] == 0, eqn[1] == 0,
     eqn[2] == 0, eqn[3] == 0, phi[s1] == phi[0] + Pi / 2, kappa[s1] == 0},
    {q1, -3.}, {q2, 10.}, {q3, 3.}, {q4, 1.}, {q5, .1}, {s1, 3.},
    WorkingPrecision → 40, AccuracyGoal → 20
   ] // Chop // SetPrecision[#, 12] &
```

```
{q1 → -3.09202344293, q2 → 11.6170264041, q3 → 3.23513331220,
 q4 → 1.25570302484, q5 → 0.133149136310, s1 → 3.42166776869}
```

FIG. 5. A minimalist solution of the end-loop equations, using WOLFRAM MATHEMATICA.

[1] A. Love, *A Treatise on the Mathematical Theory of Elasticity* (Dover, New York, 1944).
[2] L. Giomi and L. Mahadevan, Proc. R. Soc. London, Ser. A **468**, 1851 (2012).
[3] A. E. Cohen and L. Mahadevan, Proc. Natl. Acad. Sci. USA **100**, 12141 (2003).
[4] J. Bico, B. Roman, L. Moulin, and A. Boudaoud, Nature (London) **432**, 690 (2004).
[5] J. E. Flaherty, J. B. Keller, and S. I. Rubinow, SIAM J. Appl. Math. **23**, 446 (1972).
[6] J. Plateau, Mém. Acad. Roy. Belgique **29**, 1 (1849).
[7] M. Lévy, J. Math. Pure Appl. **10**, 5 (1884).
[8] G. F. Carrier, J. Math. Phys. **26**, 94 (1947).
[9] A. J. Adams, J. Math. Phys. **49**, 032902 (2008).
[10] I. Tadjbakhsh and F. Odeh, J. Math. Anal. Appl. **18**, 59 (1967).
[11] P. A. Djondjorov, V. M. Vassilev, and I. M. Mladenov, Int. J. Mech. Sci. **53**, 355 (2011).
[12] H.-Y. Kim and L. Mahadevan, J. Fluid Mech. **548**, 141 (2004).
[13] C. Py, P. Reverdy, L. Doppler, J. Bico, B. Roman, and C. N. Baroud, Phys. Rev. Lett. **98**, 156103 (2007).
[14] K. Holmberg, B. Jonsson, B. Kronberg, and B. Lindman, *Surfactants and Polymers in Aqueous Solution* (Wiley, Chichester, 2007).
[15] S. Antman, J. Math. Anal. Appl. **21**, 132 (1968).
[16] R. Burridge and J. B. Keller, SIAM Rev. **20**, 31 (1978).
[17] C. Majidi, Mech. Res. Commun. **34**, 85 (2007).
[18] Computer code WOLFRAM MATHEMATICA (Wolfram Research, Inc., Champaign, IL, 2011).